Microstructure of $YBa_2Cu_3O_{7-\delta}/Pb(Zr_{1-x}Ti_x)O_3$ (x = 0, 0.47) heterostructures

2002 J. Phys.: Condens. Matter 14 3093

(http://iopscience.iop.org/0953-8984/14/12/302)

INSTITUTE OF PHYSICS PUBLISHING JOURNAL OF PHYSICS: CONDENSED MATTER

J. Phys.: Condens. Matter **14** (2002) 3093–3097 PII: S0953-8984(02)31514-5

Microstructure of $YBa_2Cu_3O_{7-\delta}/Pb(Zr_{1-x}Ti_x)O_3$ (x = 0, 0.47) heterostructures

L X Cao[1], Y L Qin[2], A Deac[1], I Snigireva[1] and J Zegenhagen[1,3]

[1] European Synchrotron Radiation Facility, BP 220, F-38043 Grenoble Cedex, France
[2] Institut für Festkörperforschung, Forschungszentrum, Jülich GmbH, D-52425 Jülich, Germany

E-mail: zegenhagen@esrf.fr

Received 4 December 2001
Published 15 March 2002
Online at stacks.iop.org/JPhysCM/14/3093

Abstract

Epitaxial $PbZrO_3$ (PZ) and $Pb(Zr_{0.53}Ti_{0.47})O_3$ (PZT) films were prepared on epitaxial $YBa_2Cu_3O_{7-\delta}$ (YBCO) on $SrTiO_3$(001) by pulsed laser deposition. PZ was deposited at low substrate temperature followed by *in situ* oxygen annealing. Similar to PZT, the PZ grows as a dense film, but it is rougher and has more pinholes than PZT as a result of the larger lattice mismatch with YBCO. Both YBCO/PZ and YBCO/PZT heterostructures exhibit sharp interfaces, with edge dislocations located close to the interface.

In the past decade, heterostructures of ferroelectrics (FEs) integrated with high-temperature superconductors (HTSs), such as $YBa_2Cu_3O_{7-\delta}$ (YBCO), have been intensively studied [1–3]. YBCO/$Pb(Zr_{1-x}Ti_x)O_3$ ($x > 0.1$), in which YBCO serves as the electrode layer for the FE layer because of its structural and chemical similarity, were synthesized by pulsed laser deposition (PLD) [2, 4] and magnetron sputtering [5] etc. The research on FE/HTS heterostructures may benefit either ferroelectric devices, for example microelectromechanical systems, memory devices, thin-film capacitors, infrared vidicons and solid state displays, or superconducting devices such as superconducting field effect transistors. It was found that the performance of these heterostructures is strongly affected by their microstructure [3].

Antiferroelectric (AFE) $PbZrO_3$ (PZ) thin films caught some attention, too, because of their possible advantageous use in capacitors with high energy storage capacity, micro-transducers with fast response time and possible applications in terms of field-induced ferroelectricity etc. However, less work has been done on AFE heterostructures, compared with their FE counterparts. In this context, integration of PZ with *noble metals*, such as Pt, or *semiconductors*, such as Si, has been realized by the sol-gel method [6–8], sputtering [9, 10], PLD [11, 12] and metallorganic chemical vapour deposition [13]. To the best of our knowledge, there is no report so far on PZ/HTS heterostructures.

[3] Author to whom any correspondence should be addressed.

0953-8984/02/123093+05$30.00

Recently, we studied the temperature dependence of the dielectric response of YBCO/Pb($Zr_{0.53}Ti_{0.47}$)O_3 (YBCO/PZT) and YBCO/PZ heterostructures, and found a dielectric anomaly, which is related to the ferroelectricity of the PZT, at the superconducting transition of the YBCO [14]. However, from the above it is clear that more work is needed for the structural characterization of YBCO/PZT and YBCO/PZ heterostructures, especially at their interfaces. In this paper we studied microstructures of YBCO/PZT and YBCO/PZ, which we had grown by PLD, by x-ray diffraction (XRD), scanning electron microscopy (SEM), atomic force microscopy (AFM) and transmission electron microscopy (TEM).

The YBCO/PZT and YBCO/PZ heterostructures, with the PZT or PZ layer on top of the under-doped YBCO layer, were deposited on $SrTiO_3$(001) in a multi-target PLD system. A KrF excimer laser ($\lambda = 248$ nm) with a repetition rate of 1 Hz was focused with a power density of 50 mJ mm^{-2} on a rotating target, either YBCO, PZT or PZ. The sample was located 60 mm above the target, the surface of which was parallel to the sample surface. YBCO was deposited at a substrate temperature of 760 °C in an oxygen pressure of 50 Pa, then annealed for 30 min at 450 °C in 8×10^4 Pa oxygen before the heating power was switched off. Immediately afterwards the PLD chamber was pumped down to high vacuum and the PZT or the PZ layers were deposited on the YBCO layers as described below. The correspondingly chosen oxygen pressure and cooling process created the final oxygen stoichiometry in the YBCO layers[4].

Two ceramic targets, with nominal composition of $Pb_{1.05}(Zr_{0.53}Ti_{0.47})O_3$ and PZ, were used. The PZT layer was deposited at 580 °C and 12 Pa oxygen pressure, and the thus obtained YBCO/PZT heterostructure was cooled down to room temperature in the same atmosphere without oxygen annealing. For PZ layers, in order to prevent Pb loss and consequently impurity phase formation, such as ZrO_2, a low-temperature deposition process was used. The PZ layer was deposited at 300 °C and 10 Pa oxygen pressure, briefly annealed *in situ* at 655 °C in 8×10^4 Pa oxygen, and cooled down to room temperature without oxygen annealing. From our experience, it is difficult to obtain single-phase PZ films and to avoid the appearance of ZrO_2 when a higher deposition temperature is employed. These growth procedures yield high-quality integrated film structures confirmed by XRD. As shown in figure 1 only the (00ℓ) diffraction peaks of YBCO and PZT (cf figure 1(*a*)) or YBCO (00ℓ) and PZ $(h00)/(00\ell)$ (cf figure 1(*b*)), besides the peaks from the STO substrate, can be distinguished in the diffraction patterns, which are logarithmically scaled. It is obvious that *exclusively* *c*-oriented PZT or *a*- and *c*-oriented PZ films grow epitaxially on the *c*-oriented YBCO films. The oxygen concentrations in the $YBa_2Cu_3O_{7-\delta}$ layers derived from the *c*-axis lattice constants are $\delta \approx 0.5$ and 0.2 for YBCO/PZT and YBCO/PZ, respectively [15], in agreement with the oxygen concentration derived from T_c measurements [14].

The microstructure of the heterostructures influences their dielectric performance, for example the dielectric constant and dielectric loss [3]. We studied a 120 nm thick PZT and a 120 nm PZ layer, grown on a 120 nm YBCO layer, by SEM and AFM. Images are reproduced in figures 2 and 3, respectively. Both the PZT and PZ layers are dense, with isolated pinholes (cf figures 2(*a*) and (*b*)). With a value of 1.5×10^8 cm^{-2} the pinhole density in the PZ film is ∼4 times larger than that in the PZT films. AFM images (cf figure 3) show height fluctuations of ∼20 nm. The PZT grains of ∼100 nm in lateral size are connected to each other, leaving fewer disconnected surface areas, i.e. pinholes, in comparison with the PZ film. The PZ layer is rougher. Grains of ∼50 nm in lateral size form particles of ∼250 nm in lateral size.

[4] The motivation to prepare under-doped rather than optimally doped YBCO was to vary the superconducting transition temperature and thus relate the onset of superconductivity conclusively to the dielectric anomaly observed in the prepared heterostructures [14].

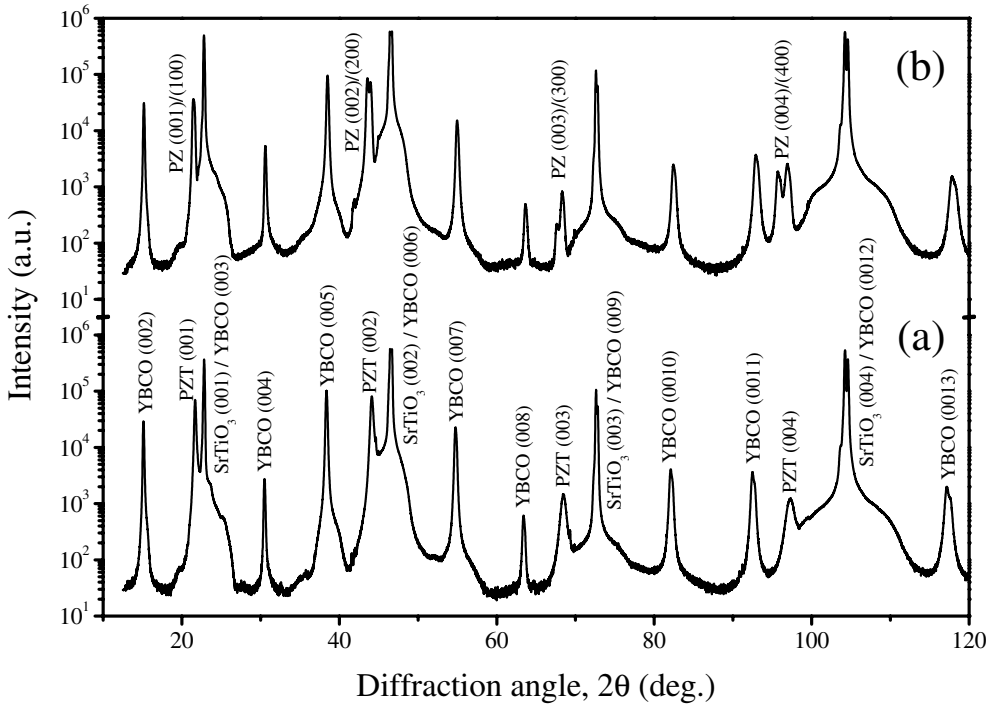

Figure 1. XRD Θ–2Θ scan for YBCO/PZT (*a*) and YBCO/PZ (*b*) on $SrTiO_3(001)$ using Cu Kα radiation. Besides peaks from $SrTiO_3$ and YBCO(00ℓ), only PZT(00ℓ) and PZ(h00)/(00ℓ) peaks can be observed. Measured lattice constants are $c_{PZT} = 0.410$ nm, $c_{YBCO} = 1.173$ nm for YBCO/PZT and $a_{PZ} = 0.416$ nm, $c_{PZ} = 0.412$ nm, $c_{YBCO} = 1.169$ nm for YBCO/PZ.

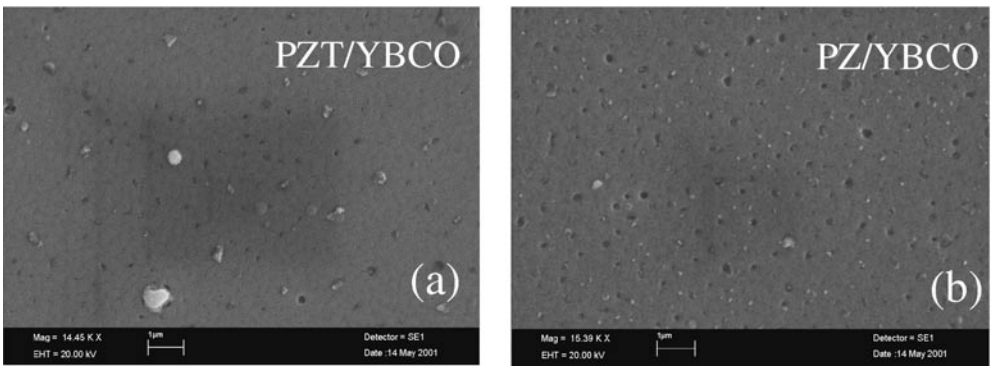

Figure 2. SEM images of PZT (*a*) and PZ (*b*) top layers of the heterostructures. The PZT film has fewer pinholes than the PZ film. The bright particles on the surfaces are not intrinsic but originate from prolonged exposure to normal ambient.

Note that the mismatch of PZ with YBCO is larger than for the PZT[5] and consequently a larger surface tension is imposed on the PZ layer. We suggest that this is responsible to the rougher morphology and the formation of pinholes in the PZ layer.

[5] The lattice constants of the bulk materials are $a_{PZT} = b_{PZT} = c_{PZT} = 0.408$ nm, $a_{PZ} = b_{PZ} = 0.415$ nm, $c_{PZ} = 0.410$ nm, $a_{YBCO} = 0.3817$ nm, $b_{YBCO} = 0.3883$ nm and $c_{YBCO} = 1.1633$ nm.

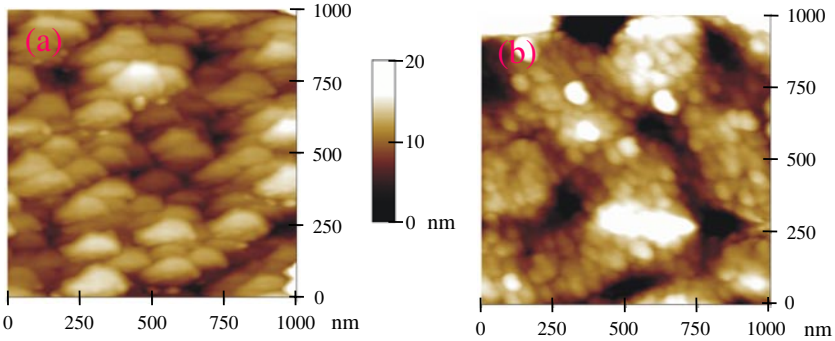

Figure 3. AFM images of PZT (*a*) and PZ (*b*) top layers of the heterostructures. The PZ film is rougher, and more pinholes can be identified on the PZ surface.
(This figure is in colour only in the electronic version)

The crystalline quality of the films strongly influences the physical properties of the heterostructures. It is believed that the poor quality of the PZT layer is one reason for the decrease of the dielectric constant in thin-film devices as compared with the bulk properties of PZT crystals [2, 3]. Thus, we analyse here a pair of YBCO/PZT and YBCO/PZ heterostructures on $SrTiO_3$(001) with 120 nm thickness for all four layers by TEM in planar and cross-sectional views. Here we show the results of cross-sectional TEM. The TEM diffraction patterns, which are reproduced in the insets of figures 1(*a*) and (*d*), show that the diffraction spots of YBCO and PZT (or PZ) are clearly separated (parallel to the interface): i.e., the heterostructures are laterally not lattice matched; they have relaxed their strain. Contrast variations in the image (figures 1(*a*) and (*d*)) along the interface can be observed in the PZT and PZ films, which appear extended in the growth direction and which are indicative of defects, which appear to be extended in the direction of the film growth (normal to the interface). Contrast variations can also be observed close to the interface, which can, however, clearly be identified. We indicated it by white arrows in the images and in the enlarged centre parts of the images of figures 4(*a*) and (*d*) (cf figures 4(*b*) and (*e*)). The transition from the YBCO layer to the PZT (or PZ) layer along the film growth direction appears sharp, without any indication of intermixing of two materials at the interface.

In order to show the interfacial dislocation network more clearly, we have Fourier filtered the TEM diffraction images (cf figures 4(*c*) and 4(*f*)). From the Fourier-transformed images only the momentum components parallel to the interface were used for the backtransformation, and therefore the lattice arrangements along the growth directions can be resolved more clearly. In these one-dimensional fringe patterns, misfit dislocations can be easily identified in the PZ, PZT and YBCO layers close to the interface. To aid recognition, we have indicated some by arrows in figures 4(*c*) and (*f*). Furthermore, anti-phase boundaries can be recognized in the YBCO layer of the YBCO/PZ sample (cf figure 4(*f*)). Above and below the boundary (marked by an oval in figure 4(*f*)), lattice planes normal to the interface are in counter-phase, i.e. shifted by half a unit cell along the direction parallel to the interface. Dislocation densities roughly $\sim 10^{12}$ cm^{-2} can be inferred from the Fourier-transformed images for the PZT and PZ layers.

In summary, PZ films integrated with *c*-oriented YBCO were prepared by low-temperature PLD and *in situ* brief oxygen annealing and compared with $SrTiO_3$/YBCO/PZT heterostructures. We found that YBCO is a good choice as the electrode layer for PZ because of its structural and chemical similarity. Both YBCO/PZ and YBCO/PZT heterostructures

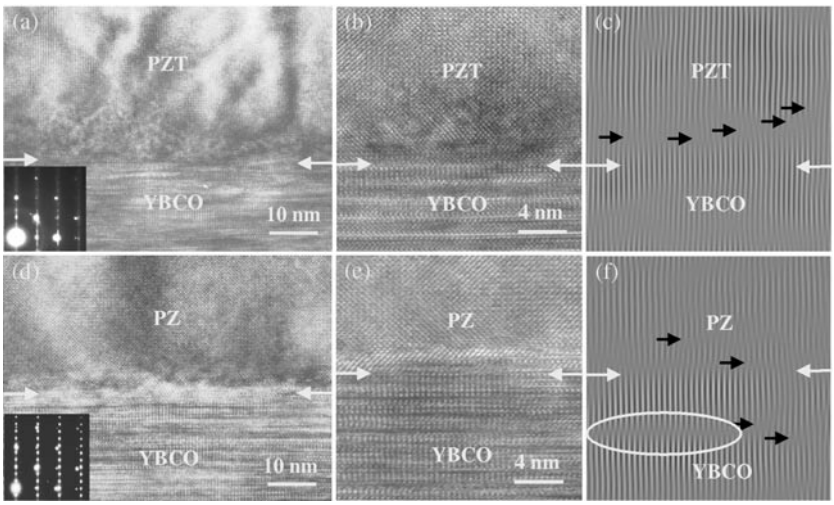

Figure 4. HRTEM images of YBCO/PZT (*a*) and YBCO/PZ (*d*) in cross-section, the insets of which are the diffraction patterns of the strain-released heterostructures. (*b*) and (*e*) are the enlargements of the centre parts in (*a*) and (*d*), respectively. The corresponding Fourier-transformed images of (*b*) and (*e*) are given in (*c*) and (*f*). White arrows denote the YBCO/PZT and YBCO/PZ interfaces. Black arrows indicate the positions of some misfit dislocations. The anti-phase boundaries in the YBCO layer are indicated by an oval in (*f*).

grown on $SrTiO_3(001)$ are single phase and epitaxial. Compared with PZT, the PZ top layer is rougher with more pinholes. Cross-sectional HRTEM clearly shows sharp interfaces of YBCO/PZ and YBCO/PZT. Dislocations are found to reside close to the interface.

References

[1] Ramesh R, Inam A, Wilkens B, Chan W K, Hart D L, Luther K and Tarascon J M 1991 *Science* **252** 944
[2] Ramesh R, Inam A, Chan W K, Tillerot F, Wilkens B, Chang C C, Sands T, Tarascon J M and Kermidas V G 1991 *Appl. Phys. Lett.* **59** 3542
[3] See, for review, Li L 2000 *Mater. Sci. Eng.* **29** 153
[4] Wu N J, Ignatiev A, Mesarwi A, Lin H, Xie K and Shih H 1993 *Japan. J. Appl. Phys.* **32** 5019
[5] Cao L X *et al* 1996 *Supercond. Sci. Technol.* **9** 310
[6] Tani T, Li J F, Vieland D and Payne D A 1994 *J. Appl. Phys.* **75** 3017
[7] Li K K, Wang F and Haertling G H 1995 *J. Mater. Sci.* **30** 1386
[8] Kong L B and Ma J 2000 *Appl. Phys. Lett.* **77** 2584
[9] Kanno I, Hayashi S, Kitagawa M, Takayama R and Hirao T 1995 *Appl. Phys. Lett.* **66** 145
[10] Yamakawa K, Trolier-McKintry S, Dougherty J P and Krupanidhi S B 1995 *Appl. Phys. Lett.* **67** 2014
[11] Chattopadhyay S, Ayyub P, Palkar V R, Multani M S, Pai S P, Purandare S C and Pinto R 1998 *J. Appl. Phys.* **83** 7808
[12] Bharadwaja S S N and Krupanidhi S B 1999 *J. Appl. Phys.* **86** 5862
[13] Bai G R, Chang H L M, Lam D J and Gao Y 1993 *Appl. Phys. Lett.* **62** 1754
[14] Cao L X, Kremer R K, Qin Y L, Brötz J, Liu J S and Zegenhagen J, submitted to *Phys. Rev.* B
[15] Jorgensen J D, Veal B W, Paulikas A P, Nowicki L J, Crabtree G W, Claus H and Kwok W K 1990 *Phys. Rev.* B **41** 1863